Sensors & Actuators: B. Chemical 424 (2025) 136923

Contents lists available at ScienceDirect

Sensors and Actuators: B. Chemical

journal homepage: www.elsevier.com/locate/snb

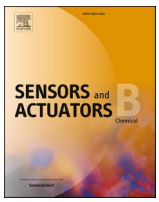

UV light-activated gas mixture sensing by ink-printed WS_2 layer

Katarzyna Drozdowska [a,*], Janusz Smulko [a], Artur Zieliński [b], Andrzej Kwiatkowski [a]

[a] Department of Metrology and Optoelectronics, Faculty of Electronics, Telecommunications, and Informatics, Gdańsk University of Technology, G. Narutowicza 11/12, Gdańsk 80-233, Poland
[b] Department of Electrochemistry, Corrosion and Materials Engineering, Gdańsk University of Technology, G. Narutowicza 11/12, Gdańsk 80-233, Poland

ARTICLE INFO

Keywords:
Gas sensors
Two-dimensional materials
Tungsten disulfide
Ink printing
Flicker noise
UV light

ABSTRACT

We fabricated a sensing layer from ink-printed WS_2 flakes and utilized it for UV-activated gas sensing. The optical imaging of the structure made by repeated printing revealed the continuous layer comprising sub-μm flakes, confirmed independently by small-area AFM images (1×1 μm^2). The activity of the sensing surface was investigated locally *via* AFM scanning of the surface with a polarized probing tip. The results indicated that the applied UV light amplifies the existing conducting paths in the dark. These hot spots are associated with the sensing activity of the WS_2 surface (local adsorption-desorption centers). Gas sensing experiments revealed that the DC resistance of the WS_2 sensor changes in the opposite direction for increasing concentrations of NO_2 and NH_3, which correlates with the electron-accepting and electron-donating properties of these species. On the contrary, low-frequency noise intensifies gradually in both gases, and relative changes in noise responses are higher than DC resistance responses for all investigated concentrations. The lowest detection limit obtained was 103 ppb from DC responses for NO_2 and 168 ppb from noise responses for NH_3. The studies of sensing responses for mixtures of the mentioned target gases revealed that the amplitude of resistance fluctuations is not a direct summation of spectra obtained for pure compounds. Such an effect observed for mixed gases indicates that the intermittent reactions between both species before adsorbing at the sensing surface or in the adsorption centers impact their detection.

1. Introduction

Gas sensors are continuously highly interesting due to numerous practical needs (safety, industry, medical diagnosis [1,2]). Two-dimensional materials (2DMs) have become an essential platform for gas sensors. Starting from graphene, 2DMs have been extensively studied recently because of their unique properties – repeatable structures of low dimensions with interesting physical properties and a high ratio of active surface to volume [3–5]. Transition metal dichalcogenides (TMDCs) belong to the group of 2DMs with the general formula MX_2, where M is the transition metal (*e.g.*, Mo, W, Nb, Ta, Zr) and X is the chalcogen atom (S, Se, Te). Those that exhibit semiconducting properties possess band gaps dependent on the number of stacked monolayers [6]. Thus, their physical and optoelectronic properties can be tuned on the fabrication level and adjusted to the desired applications, which is impossible in graphene. Apart from the numerous advantages of 2D materials, sensors based on graphene or TMDCs reported up-to-date exhibit some serious shortcomings. These include complex and expensive fabrication procedures, the need to functionalize the main material to increase its selectivity, slow responsivity, limited recovery at ambient conditions and the problem with cross-sensitivity and distinguishing between different gases when they produce similar magnitude of sensing responses.

Among TMDCs, MoS_2 is the leading representative observed to have attractive properties for gas detection, including light-assisted sensing [7–9]. Both visible light (corresponding to the optical band gap) and ultraviolet (UV) light were reported to enhance the gas-sensing properties of MoS_2 [10,11]. Since investigations on MoS_2 were promising for the fabrication of sensors, studies on other semiconducting TMDCs have recently started to develop. Tungsten disulfide (WS_2) is another two-dimensional (2D) semiconductor potentially used as a gas-sensitive part of the conductometric sensors. Its bandgap is higher than the MoS_2 mentioned above, and, therefore, it can be even more promising for some gas sensing because of the possibility of more intense energy barrier modulations (*e.g.*, by light irradiation [12]). This material is still less investigated for gas sensing applications than other 2DMs. Therefore, the experimental studies are attractive for a better understanding gas sensing mechanisms and can result in enhanced sensing properties

* Corresponding author.
E-mail address: katarzyna.drozdowska@pg.edu.pl (K. Drozdowska).

https://doi.org/10.1016/j.snb.2024.136923
Received 1 August 2024; Received in revised form 7 October 2024; Accepted 9 November 2024
Available online 12 November 2024

and potentially new applications. Similarly to MoS_2, the band gap of WS_2 increases with the decreasing number of layers, going from ~1 eV in the bulk to ~2 eV in the monolayered form while also changing from indirect to direct gap [13,14]. 2D WS_2 usually exhibits *p*-type conductivity; however, it was recently presented that its *n/p* property can be tuned using different fabrication methods. For instance, a drop-coated film comprising WS_2 flakes exhibited *p*-type conductivity, whereas inkjet-printed layers showed *n*-type behavior due to the interaction of the ink with an inert carrier gas (N_2) during printing [15]. In general, solution processing followed by various coating and printing techniques, employed initially mainly for depositing organic materials, has become increasingly common for producing gas-sensitive layers from different 2D structures [16–18]. Ink printing from solution with 2D flakes dispersed in the selected solvent requires less complex apparatus than chemical vapor deposition and less labor-demanding than mechanical exfoliation while preserving high production yield at low cost [19]. Ink-printed layers consisting of overlapping 2D flakes can provide multiple adsorption sites, particularly edges and connection spots between nanoflakes. Incident light can additionally create binding sites during the photoactivation of the sensing surface. S. Noyce *et al.* investigated a single atomic layer of MoS_2 incorporated in a field-effect transistor *via* atomic force microscopy with a customized tip polarized with a selected voltage bias [20]. The authors mapped the electrical activity of the channel with MoS_2 monolayer and discovered specific hot spots whose activity increased with increasing voltage between the FET channel and the mapping tip. The intriguing but not yet explored issue is how light activation affects the hot spots in the 2D structure and how it can be related to gas adsorption. Mapping the sensitivity of printed WS_2 layers utilized in light-assisted gas sensors can be crucial to understanding light-driven detection by ink-printed devices.

Ink-printed layers consist of multiple structures, so their specific morphology can result in lower sensitivity and selectivity than individual single-atomic layers because electron hopping between the flakes reduces the semiconducting character of the WS_2 single-atom layer. Monitoring changes in DC resistance is the primary way to measure responses to gases induced in resistive sensors. However, low-frequency resistance fluctuations (fluctuation-enhanced sensing – FES) can also provide valuable information for gas detection [21]. The FES manifested its utility in discriminating between some organic vapors by graphene-FET [13] or identifying NO_2 concentrations by carbon nanotube networks [22]. Processes of charge trapping and scattering occurring during molecular adsorption/desorption induce fluctuations in the resistance of the gas-sensitive material [23]. The limited research on employing the FES method for light-enhanced gas sensors by 2D materials leaves room for original discoveries, especially for detecting mixtures of different gases by a single sensor and studying the effect of their cross-sensitivity – the practical problem that needs fixing. These issues are addressed in our studies, trying to explain the existing research gap when a low-cost gas sensor operating at RT is proposed.

This work demonstrates a resistive sensor with the ink-printed layer comprising WS_2 flakes studied in the atmosphere of two gases of opposite redox properties. The measurement methodology includes collecting DC resistance responses in time and resistance fluctuations spectra in the low-frequency range (1–800 Hz) under selected ambient conditions. Electrical AFM investigated the effect of UV light activation of the WS_2 layer, which confirmed that UV irradiation locally enhanced conductivity in the structure of overlapping WS_2 flakes. The UV-assisted sensor was studied in different ambient gases, including the mixtures of nitrogen dioxide (NO_2) and ammonia (NH_3), which unraveled the specificity and complexity of detecting two crossing gases with distinct resistance and noise features. This way, we demonstrate the utility of the FES method toward mixed concentrations of gases detected by UV-enhanced ink-printed sensors. Additionally, mapping of the sensing surface activity employing AFM supports understanding the effect induced by UV light. Irradiation creates (or amplifies) hot spots of enhanced carrier transport properties, which locally increases the number of binding sites exploitable during molecular adsorption. Our work emphasizes the methodology of utilizing DC resistance monitoring with FES for UV-enhanced printed gas sensors based on WS_2 flakes. By simplifying the fabrication of the WS_2-based sensors and introducing the FES method and machine learning for differentiating between target species, we point toward low-cost devices for NO_2 and NH_3 detection (including mixtures of these gases).

2. Experimental section

2.1. Ink-printed sensors fabrication

WS_2 flakes dispersed in ethanol-water solution (concentration of flakes = 26 mg/L) were purchased from Graphene Supermarket and used as ink to print gas sensing layers. The lateral size of flakes is 50–150 nm, and their thickness is 1–4 monolayers. The structural and optical characteristics of pristine WS_2 flakes, including SEM image, UV–vis absorption spectrum, Raman spectrum, and depiction of the crystal structure, can be found on the producer's website (www.graphene-supermarket.com). Ceramic (Al_2O_3) platforms from Tesla (type KBI2) were used as substrates for WS_2 flakes deposition. Each sensing substrate has a platinum interdigitated electrodes structure (IDES) of line/gap width of 15/15 μm. More details on the used ceramic substrates can be found on the producer's website (www.tesla-blatna.cz).

Prior to ink printing of WS_2 layers, ceramic substrates were ultrasonically cleaned in isopropanol and acetone and cleansed with deionized water. The solution with WS_2 nanoflakes was subjected to sonication for 30 minutes to ensure no aggregates. Printing of the sensing layer was realized using Nordson Precision Fluid Dispenser (type Ultimus Plus II). Droplets covering the whole IDES were formed using the needle tip of the inner diameter of 610 μm. The time of releasing a single droplet was 0.05 s, and the carrier gas (N_2) pressure was 0.04 bar. Printing repetitions were performed ten times to ensure the continuity of the printed layer between the electrodes. After the deposition of each droplet, the material was dried in airflow (~50 °C) to evaporate the residuals of the solvent. The same printing procedure was performed to obtain WS_2 layers on Si/SiO_2 for optical imaging and on glass substrates with deposited Au layer for electrical AFM imaging. The photographs of the printing station and WS_2 sensor with the scheme of the printing process are demonstrated in Fig. A1.

2.2. Optical, electrical, and flicker noise measurements

Optical imaging of the printed WS_2 flakes was performed using a Delta Optical MET-1000-TRF microscope with up to 1000x magnification. AFM imaging (topographic and current) was realized using the Ntegra Prima atomic force microscope manufactured by NT-MDT (Russia). For contact mode scanning (by-sample mode), a CSG10Pt probe manufactured by NT-MDT was utilized. The probe was characterized by the following geometric parameters: cantilever length 225 ±5 μm, width 30±5 μm, thickness 0.5±1.5 μm, tip curvature radius 15–20 nm, the thickness of Pt conductive tip coating was 20–30 nm. The value of the spring constant (k = 0.1 N/m) was determined by the Sader method and corresponded to the contact force of 12 nN. The current flow was caused by applying a voltage of 5 V transversely to the applied layer. Scanning was performed at a speed of 1.01 μm/s, corresponding to spatial resolution of 3.92 nm. UV irradiation was realized using the same LED, type PB2D-1CLA-TC (wavelength of 275 nm and optical power density of 1.59 mW/cm^2) as for other measurements. The TS-150 active anti-vibration table was also part of the vibration-damping system.

For electrical and low-frequency noise measurements, IDES terminals of the sensor were connected with the measuring and biasing units *via* the Teflon board to reduce eventual leakage currents. The sensor was connected in series with the loading resistor of R = 478 kΩ (having a similar magnitude to the sensor resistance). Keysight E3648A DC power supplier was used to polarize the sensor and the resistor. Time-resolved

measurements were conducted at 20 V bias, resulting in 6–10 V across the sensor. Low-frequency noise measurements were performed using the same circuit with two accumulators. Noise spectra were collected with a signal analyzer (Stanford Research Systems, model SR785), and the signal was amplified using a low-noise voltage amplifier (Stanford Research Systems, model SR560). The sensing chamber, batteries, and voltage amplifier were put inside a grounded metal shielding box covered with an amorphous cobalt foil, type MCF5 YSHIELD® (yshield.com), to reduce external noise interferences at low frequencies, the effect of ambient light, laboratory airflow, and ambient temperature changes. The sensing responses were monitored in the dark and under UV light (275 nm, 1.59 mW/cm^2). UV LED was positioned close to the sensing surface (less than 0.5 cm).

The circuit used for DC and noise measurements utilized the voltage divider (sensor R_S in series with resistor R), so R_S was calculated as $(V_S \cdot R)/(V_0 - V_S)$, where V_S is the measured voltage across the sensor, and R and V_0 are 478 kΩ and 20 V, respectively. Similarly, the measured voltage fluctuations (power spectral density of voltage fluctuations, S_V) were converted into power spectral density of resistance fluctuations S_R by following dependence: $S_R/R_S^2 = S_V/V_0^2 \cdot [(R+R_S)^2/(R \cdot R_S)^2]$, as presented elsewhere [24]. The detection limit (DL) was calculated based on changes in the sensor resistance in time or the average noise spectrum in the selected frequency range (2–20 Hz). The procedure for DL estimation is described in detail in Supplementary Material.

2.3. Gas-sensing experiments

We selected nitrogen dioxide (NO_2) and ammonia (NH_3) as target gases due to their opposite redox properties. Both gases are harmful to the environment and humans at concentrations of single ppm and below and are relevant for studying the effect of cross-sensitivity. Dry synthetic air (S.A.) was used as a carrier gas and a reference atmosphere. To obtain selected concentrations of target gases, we mixed S.A. with calibrating gases (20 ppm of NO_2 diluted in S.A. or 30 ppm of NH_3 diluted in N_2) at specific proportions. We maintained a constant overall gas flow of 50 mL/min regulated by mass flow controllers (Analyt-MTC, model GFC17). Sensing experiments were conducted at room temperature (RT ~25 °C) and ambient pressure (~1 bar). For experiments with a humid atmosphere, relative humidity (RH) of 40 % was produced by transferring 50 mL/min of S.A. through the container with deionized water before mixing with target gases and reaching the sensing surface.

3. Results and discussion

An optical image of the ink-printed layer (Fig. 1a) indicates that WS_2 flakes formed a continuous film on the micrometer level after ten printing repetitions. Printing sensing layers from inks with low-viscosity solvents (*e.g.*, ethanol) usually leads to the coffee-ring effect at the edges of the released droplet, formed due to the faster evaporation of the solvent at the droplet edge than in its center [16]. Comparing optical images in the center and at the edge of the deposited WS_2 layer (Fig. A2), the discontinuity starts to be visible in some parts of the film, around 50–60 μm from the outer edge of the droplet. To avoid the inhomogeneity of the sensing layer printed on Pt electrodes (inset in Fig. 1a), the printing parameters were adjusted to form a droplet covering a larger area than only the IDES part of the ceramic substrate.

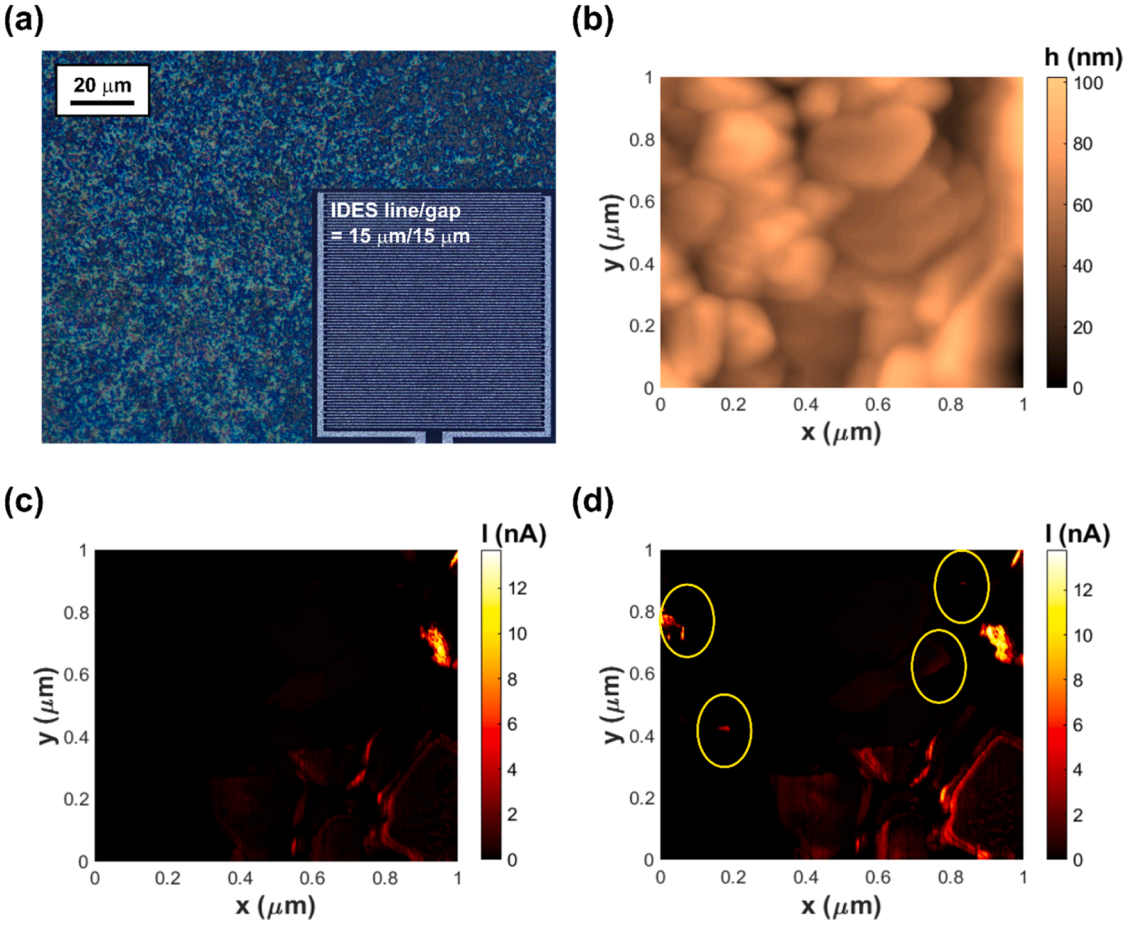

Fig. 1. **(a)** Optical image of the WS_2 layer under 500x magnification (the scale bar is 20 μm) printed on a ceramic substrate with IDES of line/gap of 15/15 μm (the picture of the substrate under 50x magnification in the inset). **(b)** An AFM image of the WS_2 layer obtained after ten printing repetitions. An AFM image in the electrical mode for **(c)** non-irradiated sample and **(d)** for the same area irradiated with UV light. The yellow ovals indicate UV-activated areas.

The percolation path was provided by flakes overlapping each other after multiple printing repetitions. AFM image of the WS_2 layer shows that the thin film consists of aggregated sub-μm flakes, and the structure height varies at around tens of nanometers (Fig. 1b). The thickness of the ink-printed WS_2 layer measured locally with a profilometer was 50 nm on average, which agrees with the AFM imaging results. WS_2 thin film printed on the glass substrate with an Au conducting layer was used to map the electrical activity of the sensing surface by a polarized AFM probe. The current flowing from the conducting substrate to the probing tip through the WS_2 layer was measured locally, revealing some electrically active spots corresponding primarily to the edges of the agglomerated nanoflakes (Fig. 1c). These hot spots provide charge transfer through the printed layer and can be correlated with the localized surface activity of the resistive gas sensor. After irradiation with UV light, the activity of spots visible in the dark was magnified, and a few appeared in new locations. Yellow ovals in Fig. 1d highlight the hot spots visible only after irradiating the structure with UV light. Notably, photoactivation of the WS_2 layer occurs non-homogeneously; however, UV light activates the surface and increases charge transfer through the printed structure by photoinduced charge carriers. Such surface activation can be beneficial for enhanced gas detection based on surface adsorption and charge transfer between molecules and the sensing surface.

We started gas sensing experiments by comparing the repeatability of DC resistance responses to NO_2 and NH_3 in the dark and under UV light. Fig. 2 shows that sensor resistance R_S varies between about 0.1 and 0.4 MΩ depending on the ambient gas and irradiation conditions when the voltage across the sensor was set between 6–10 V. The voltage divider was supplied with a voltage $V_0 = 20$ V. We opted for >6 V across the sensor to obtain the stable baseline; however, we observed that the relative change in the sensor resistance induced by UV light or target gas was the same regardless of the voltage supply (reduced to even 1 V), despite the semiconducting character of the WS_2 layer. Thus, we believe the voltage supply could be reduced at least a few times, which offers low power consumption while maintaining the sensor responsivity. Sensor baseline resistance in S.A. decreased almost twice, which can be explained by the effect of UV irradiation that cleans the surface from the adsorbed oxygen and humidity. The anti-humidity effect was observed before for UV-assisted WS_2/PbS heterostructure [25] and is a well-established effect for UV-irradiated sensors composed of low-dimensional materials [26,27]. Five consecutive cycles of introducing 5 ppm of NO_2 or NH_3 resulted in repeatable responses with the absolute changes in R_S higher for the irradiated sensor (almost two times for NO_2 and more than three times for NH_3). R_S increases in the presence of NO_2 and decreases for NH_3, as these gases exhibit opposite oxidizing/reducing properties. NO_2 is an electron-accepting molecule that captures electrons from the conduction band of WS_2. NO_2 adsorption increasing sensor resistance indicates that the WS_2 layer behaves as an *n*-type semiconductor. This is confirmed by the decreasing resistance after the adsorption of NH_3, an electron-donating compound. Such semiconducting behavior is less common for WS_2 flakes of nanoscale dimensions as this material usually exhibits *p*-type conductivity in the low-dimensional form. Nevertheless, *n*-type conductivity has been reported recently for printed WS_2 layers, indicating that the fabrication

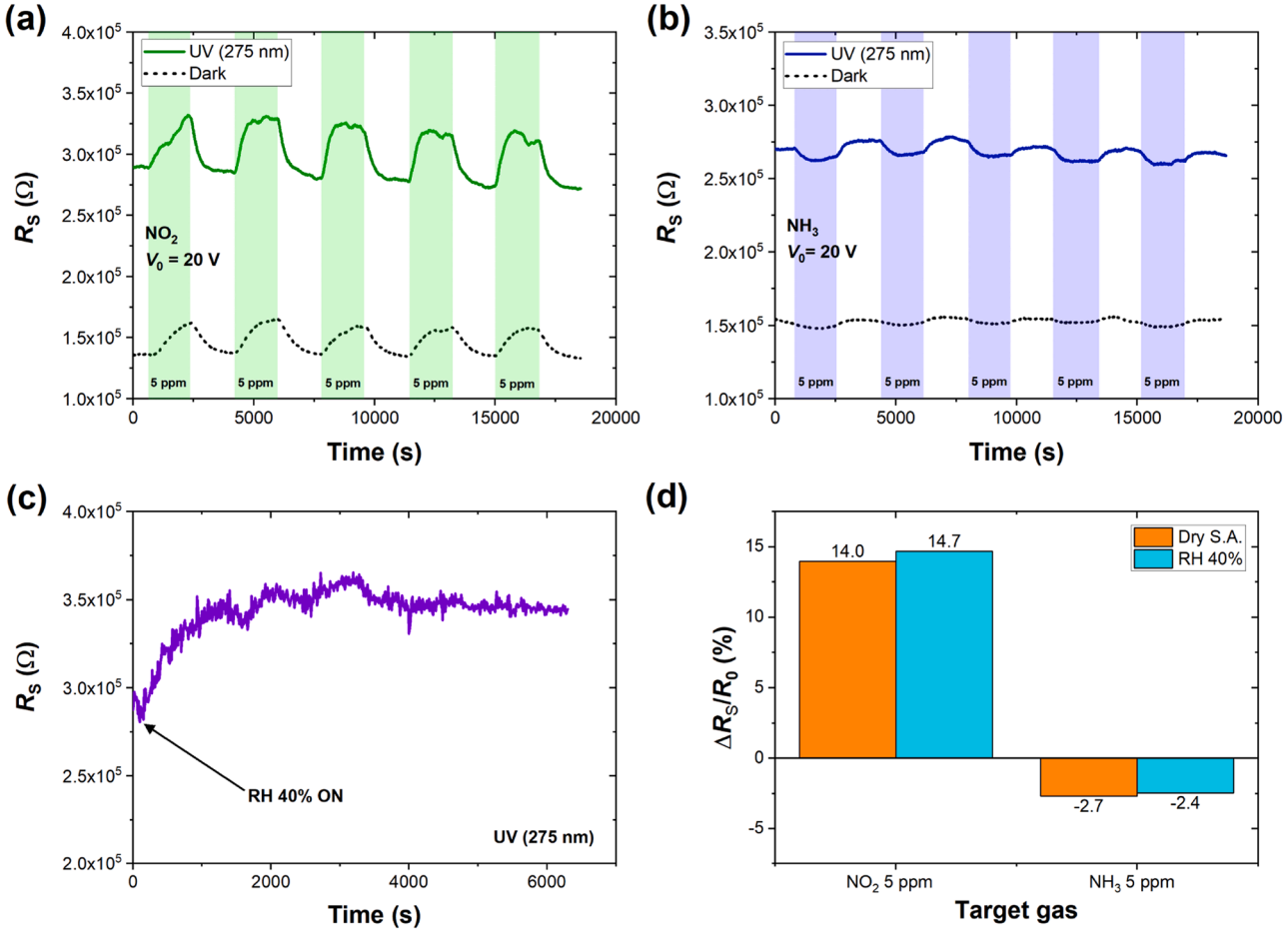

Fig. 2. Time-resolved measurements (sensor resistance R_S) of the ink-printed WS_2 sensor in the dark and under UV light (275 nm) for five consecutive cycles of **(a)** 5 ppm NO_2 and **(b)** 5 ppm NH_3 introduction. The voltage bias $V_0 = 20$ V. The effect of RH 40 % **(c)** on the sensor resistance baseline and **(d)** on responses to 5 ppm of NO_2 and NH_3 under UV irradiation. The value for dry S.A. conditions was derived as an average response from five cycles presented in **(a)** and **(b)**.

process can be adjusted to tune the *n/p* semiconducting properties of this material [15]. We estimated the response and recovery times based on cycles from Fig. 2a (NO_2) and Fig. 2b (NH_3) as an average value from five consecutive detection cycles. We define the response and recovery time as the time required for the sensor to reach 90 % of the saturated response/recovery. In the case of NO_2, the average response time was 1218 s in the dark and almost two times shorter – 656 s under UV light, whereas the recovery time was 1122 s in the dark and only 450 s under irradiation. For NH_3, the response/recovery time was 874/908 s in the dark and 630/646 s under UV light, showing an enhancement in the speed of operation for both investigated gases when the sensing surface is irradiated.

We also tested the effect of relative humidity (RH) on sensing responses. We utilized humid air of RH = 40 % and measured how the sensing baseline stabilized in time. In Fig. 2c, we notice that a humid atmosphere increases the sensor resistance by ~20 % in the first 30 minutes, and then the baseline stabilizes. Moreover, we tested whether such humid air changes the sensor responsivity to NO_2 and NH_3. Fig. 2d compares the relative changes in sensor resistance obtained in dry and humid S.A., which are close in values. Notably, in our measurements, we reduce the effect of humidity by utilizing irradiation with UV light. Water molecules occupy some adsorption/desorption centers, but UV irradiation assures sufficient binding sites for investigated gases. Thus, the responses to NO_2 and NH_3 are similar, at least for RH ~40 % (the typical value for indoor ambiance). Therefore, we focused on studying sensing responses in dry S.A. for further experiments with varied and mixed concentrations of NO_2 and NH_3. We also want to notice that the sensor baseline resistance was stable and remained at similar levels after irradiation with UV light (~300 kΩ) for more than nine months. The sensor also maintained its responsivity to two investigated gases (NO_2 and NH_3) and their mixtures over a few months of exploitation. We observed that the sensor DC resistance stabilizes under UV light after polarizing the sample, and the irradiation time can be modulated and extended if necessary when the sensor remained in the ambient conditions for longer or aged.

Next, we tested the sensor responsivity to selected concentrations of target gases under UV light. Fig. 3 depicts the results of the quantitative detection of NO_2 and NH_3 (1–10 ppm) established as the relative changes in the sensor resistance, where the reference condition was baseline resistance R_0 at the beginning of each measurement (Time = 0 from the corresponding graphs). The results demonstrate that NO_2 induces more significant changes in R_S than NH_3, presumably ascribed to the higher adsorption energy of NO_2. Thus, 10 ppm of NO_2 changes R_S to 20 %, whereas the same ammonia concentration induces a resistance decrease of less than 10 %. We also tested if the sensor responds to other gases, *e.g.,* organic ethanol. DC resistance measurements with 110 ppm of ethanol revealed a response of ~68 %. It signals that the WS_2 sensor has limited selectivity and can be highly sensitive to various gases; therefore, an extended methodology of measurements and data analysis are required to utilize the unmodified ink-printed WS_2 layers as gas sensors in practical applications.

Apart from the sensor DC resistance in selected atmospheres, the random resistance component can provide information about the detected gases and their concentrations. Fig. 4 summarizes the noise spectra collected for selected concentrations of NO_2 and NH_3 (1–10 ppm) in the dark and under UV light. WS_2 sensor exhibits $1/f$-like noise in the investigated frequency range, and the noise intensity gradually increases with the increasing concentration of both gases. The lack of distinct Lorenztian components in the spectrum indicates that the observed noise is most likely generated by multiple trapping states over a wide range of relaxation times. Then, the ultimate low-frequency noise spectrum is the summation of numerous events of different lifetimes observed in semiconductors [28].

Fig. 5 shows the product of normalized power spectral density of resistance fluctuations and the frequency $S_R(f)/R^2 \times f$. A concentration of 1 ppm induced a minor effect close to the S.A. case for both species. Producing the concentration of 1 ppm was burdened with a significant error due to limitations of the utilized gas calibration system, so this point was omitted in the subsequent analysis of noise responses. The data points in Fig. 5 correspond to the average value from the 2–20 Hz frequency range, selected as the most informative noise bandwidth preserving linear dependence with gas concentration increase, and show the differences between the noise amplitude in the dark and under UV light. The change in $S_R(f)/R_S^2 \times f$ due to increasing gas concentrations follows a linear dependence. In the case of all concentrations of NH_3, the variation between dark and light-enhanced conditions is minor. For NO_2, the differences start to be more apparent for higher concentrations, over 2 ppm. In this case, the change in the noise amplitude is steeper for the UV-irradiated sensor. Even though NO_2 and NH_3 produce opposite changes in sensor DC resistance, the adsorption of both gases causes increased resistance fluctuations. The adsorbed molecules act as scattering centers for charge carriers, like additional surface defects, increasing flicker noise intensity with the number of adsorbed/desorbed molecules (increased gas concentration).

The dependence between the relative change in DC resistance or noise amplitude and concentration of target gases informs about the sensitivity of the investigated WS_2 gas sensor. Fig. 6 presents the relative changes in sensor DC resistance or normalized power spectral density of resistance fluctuations multiplied by f in reference to the case of S.A. Detection limits (DLs) for NO_2 and NH_3 were calculated separately for

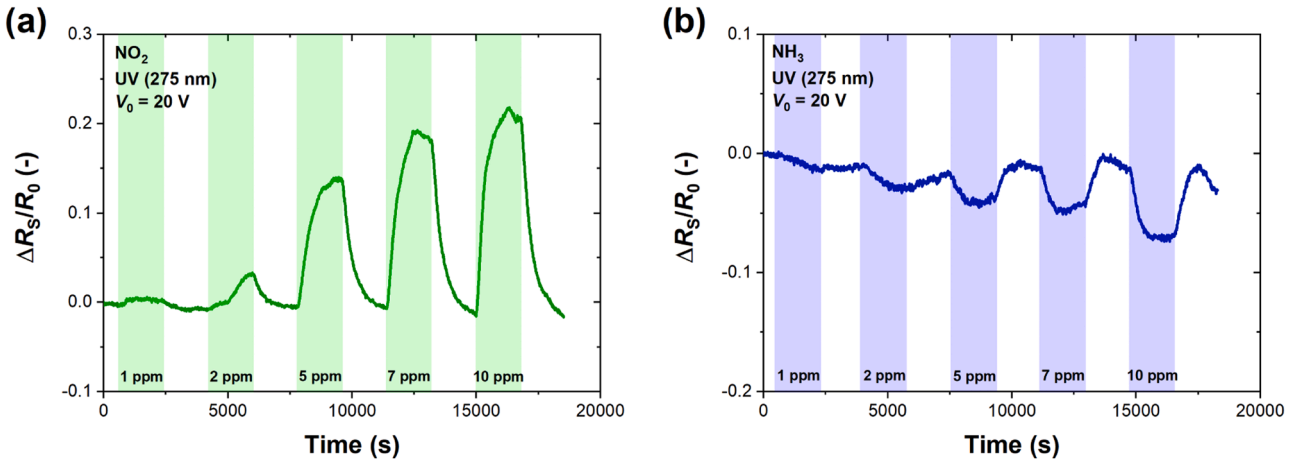

Fig. 3. Time-resolved measurements (relative change of sensor resistance ΔR_S in reference to R_0 in S.A.) of the ink-printed WS_2 sensor under UV light (275 nm) for **(a)** 1–10 ppm NO_2 and **(b)** 1–10 ppm NH_3. The voltage bias V_0 = 20 V.

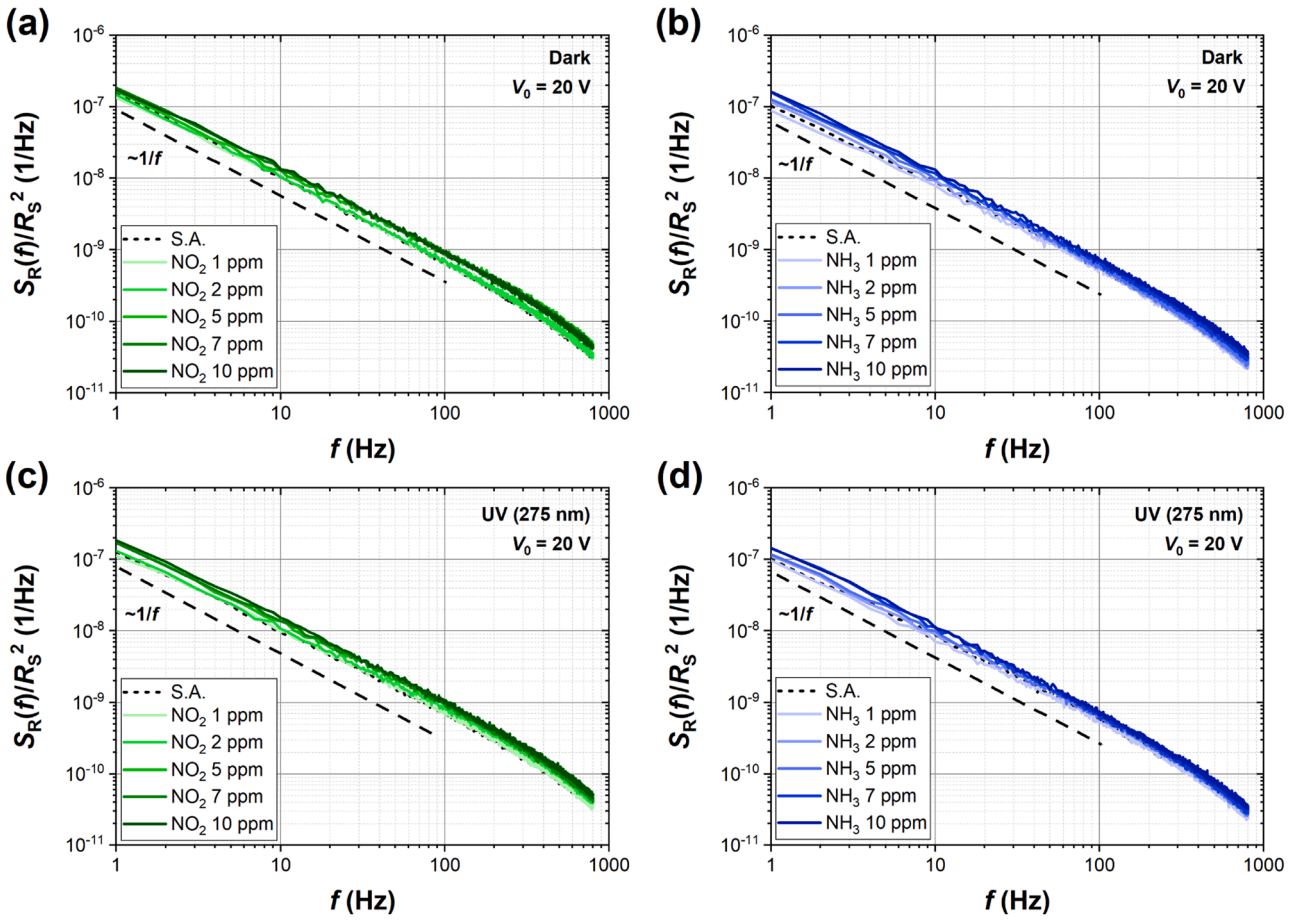

Fig. 4. Power spectral density of resistance fluctuations S_R normalized to the square of sensor resistance R_S^2 measured between 1–800 Hz for selected concentrations of NO_2: **(a)** – in the dark and **(c)** – under UV light (275 nm); and NH_3: **(b)** – in the dark and **(d)** – under UV light (275 nm). Dashed lines marked on the graphs follow the $1/f$-like dependence. The voltage bias $V_0 = 20$ V.

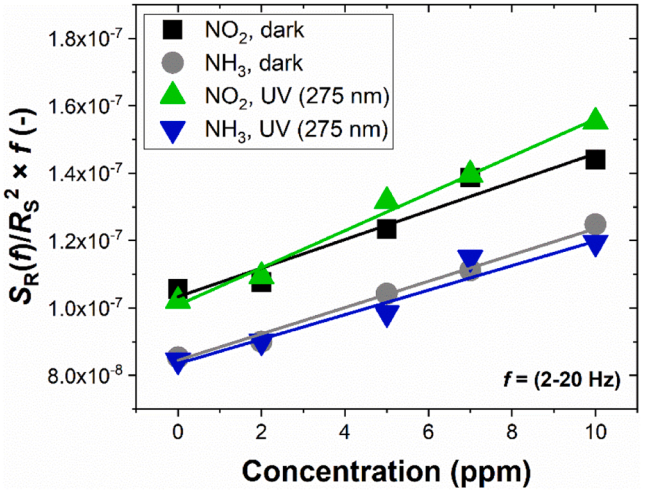

Fig. 5. The product of normalized power spectral density of resistance fluctuations $S_R(f)/R_S^2$ and frequency f as an averaged value in the range 2–20 Hz for NO_2 and NH_3 in the dark and under UV light (275 nm).

DC resistance and noise data. For NO_2, DL was estimated as 103 ppb from DC resistance responses and 220 ppb from noise responses. Additional DC resistance measurements with NO_2 of lower concentrations (50–500 ppb) showed that the WS_2 sensor is responsive to concentrations at ppb level for this gas (see Fig. A3). Theoretical DL estimated for data points obtained in the low-concentration range was only 6 ppb, showing a potential of the printed sensor working with high-sensitivity when the high-accuracy measuring equipment is used. Even though lower DL was obtained from DC measurements, the noise responses were approximately two times higher for all concentrations. For instance, adsorption of 10 ppm of NO_2 resulted in the growth in sensor resistance by 22 %, but the average noise intensity increased by 52 %. The difference between resistance and noise responses is even more apparent for NH_3. For 10 ppm of ammonia, resistance change was only 7 %, whereas the noise intensity increased by 41 %, which is almost six times higher. Moreover, DL estimated using noise measurements was reduced to 168 ppb for NH_3. The results of DL estimation are biased by lower accuracy of noise measurements due to random error of the estimated power spectral density (averaging within 400 spectra, each at observation time = 1 s, supports the reduction of the random error to 5 %). Moreover, the method of DL estimation has additional limitations in the case of nonlinear sensor response. The corresponding DL values can be much better when we only apply more accurate noise measurement results and the range of DC resistance changes versus gas concentration to its linear dependence. These factors will reduce the RMS value estimated for the noise data and result in lower DL values.

The effect of cross-sensitivity to various gases of different sensing materials is a challenge for producing highly efficient devices – sensors able to detect gas mixture components. Although the selectivity to particular analytes can be improved through surface functionalization or fabricating hybrid structures and, therefore, can limit the effect of background species, the cross-reactivity of sensors based on 2D materials requires broader studies. Two target gases investigated in this work

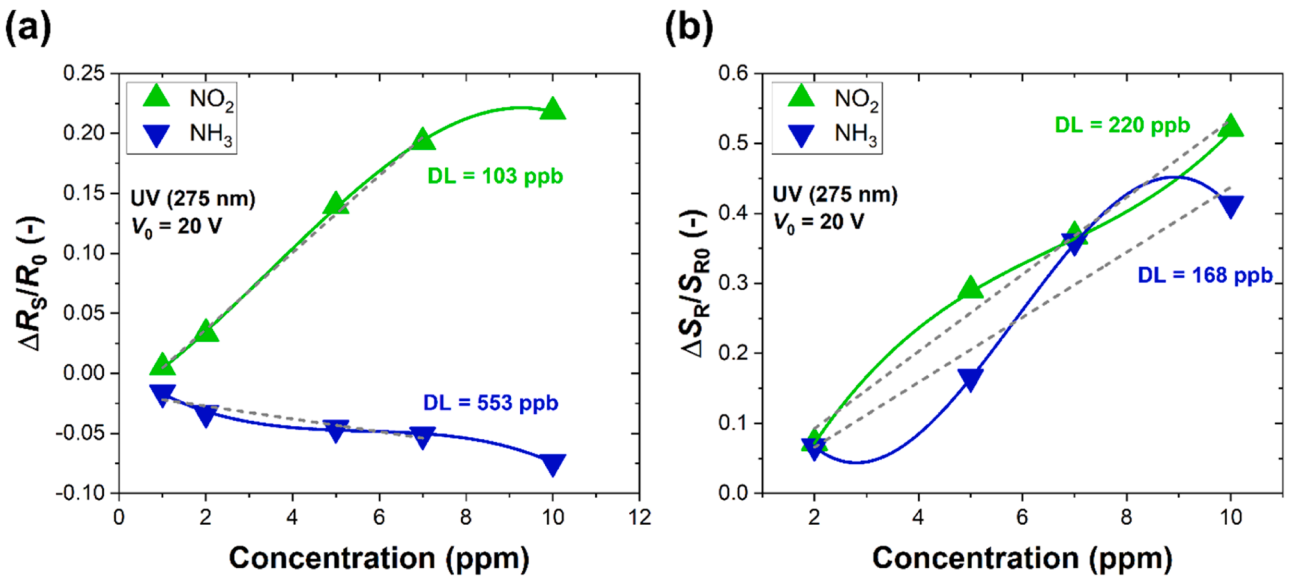

Fig. 6. Dependence between the concentration of the target gases and the relative change of **(a)** sensor resistance ΔR_S in reference to R_0 in S.A. or **(b)** normalized power spectral density of resistance fluctuations multiplied by f as the average value in the 2–20 Hz range ΔS_R in reference to S_{R0} in S.A. Solid curves refer to the polynomial functions fitted to the experimental data points, and dashed lines are linear fits used to estimate detection limits.

are common toxic species occurring in the ambient air at varied concentrations due to automotive and industrial processes (NO_2) or agricultural sector (NH_3). Thus, the sensor operating in the real-life scenario is highly likely to be affected by both gases simultaneously. Therefore, we studied the effect of their mixed concentrations on the ink-printed WS_2 sensor and compared noise and resistive responses to selected mixtures. Fig. 7 presents three-dimensional graphs summarizing the relative changes induced in sensor DC resistance and its random fluctuations by concentrations of pure and mixed gases. Data points for relative changes in noise were derived from the low-frequency noise spectra demonstrated in Fig. A4. Measurements of selected concentrations of pure NO_2 or NH_3 gases confirm that both gases produce changes in DC resistance in opposite directions. Still, the direction of changes in noise spectra with increasing gas concentration is the same for the considered gases of opposite redox properties (see Fig. A5).

Moreover, NO_2 generates a few times higher DC resistance responses than NH_3, but both gases affect the low-frequency noise spectra in the same magnitude for their considered concentrations. Interestingly, the relative changes in resistance fluctuations are not a direct summation of the noise amplitude of both gases in the case of the mixtures. Instead, all data points obtained for mixed concentrations are between or below those obtained for pure NO_2 and NH_3. Another intriguing observation is that most of the DC resistance responses are negative for mixed concentrations, even though the electron-accepting NO_2 was observed to

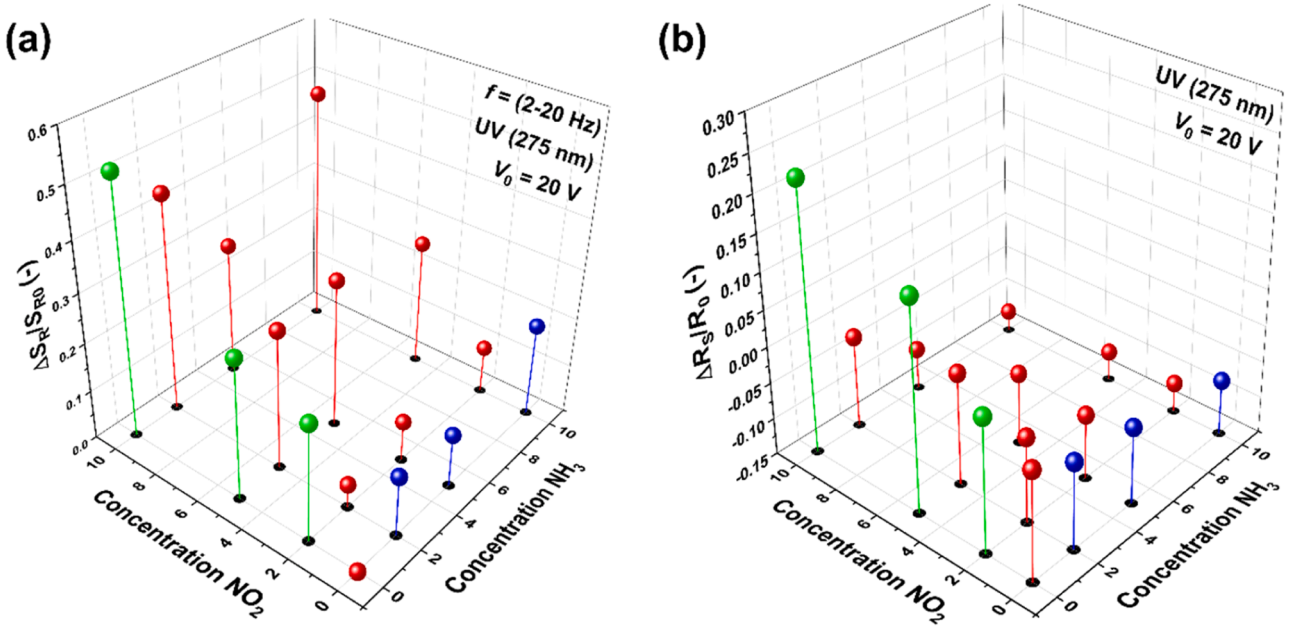

Fig. 7. **(a)** Relative change in the average value of $S_R(f)/R_S^2 \times f$ (in the range 2–20 Hz) at specific target gases (ΔS_R) in reference to the corresponding value in S.A. (S_{R0}) and **(b)** relative change in the sensor resistance (ΔR_S) in reference to the corresponding value in S.A. (R_0). The measurements were performed under UV light (275 nm) and at a voltage bias $V_0 = 20$ V. Green and blue points refer to pure NO_2 or NH_3 concentrations, whereas red points depict their mixtures and S.A. case. Black points are the X-Y projection of the 3D points for guidance and easier analysis of the results.

produce higher relative changes in sensor resistance when it remained the only target gas and was expected to dominate the sensor responsivity. In this case, it looks like NH_3 has the dominant effect on DC resistance when both gases are mixed. The partial suppression of low-frequency noise and DC responses not being exact resultant quantities in the case of mixtures suggest more complex sensing mechanisms and processes occurring at or close to the sensing surface of WS_2 flakes. These effects can be explained by interactions between the molecules of the considered gases, creating distinct responses and affecting charge transfer at the sensing interface in a particular way. We also performed dynamic sensing studies to see the direction of changes in the DC resistance when NO_2 and NH_3 of selected concentrations are introduced simultaneously. Fig. A6 shows how the sensor resistance changes in the 30-minute cycles of mixture introduction. It confirms that for small concentration of NH_3 (2 ppm), NO_2 dominates the response, especially in the first minutes. On the other hand, when 5 or 10 ppm of NH_3 is admitted to the sensing surface, the reducing gas starts to decrease sensor resistance. It signifies that after longer exposure to both gases, NH_3 can dominate the DC resistance, whereas NO_2 provides an immediate and dominant effect in the first minutes of the detection cycle. The detailed explanation of the observed gas-crossing effects requires more in-depth studies. Additionally, we suppose these mechanisms can only be characteristic of the considered gases and can be modified at different concentrations. Some reactions should occur at the gas sensing layer but in the ambient gas mixture, depending on gas concentrations and the probability of occurrence.

The presented detection data confirm that a single ink-printed WS_2 sensor can detect two toxic gases, namely NO_2 and NH_3, when only one is present in the ambient atmosphere. The change of DC resistance (Fig. 3) compared with the recorded one at the ambient atmosphere of S. A. determines which gas was introduced. Then, the intensity of flicker noise can be used to determine gas concentrations by considering the linear dependence presented in Fig. 5. This situation is similar to that presented elsewhere [29] but with much better gas sensitivity observed for the proposed ink-printed WS_2 sensor.

When we consider the data recorded for the investigated gas mixture of NO_2 and NH_3, the detection results by the studied single sensor of two gas components are less vivid. The data (Fig. 7) report an ambiguous behavior of the sensor at selected gas mixture compositions. The observed flicker noise changes (Fig. 7a) were determined mainly by NO_2 concentrations. The presence of NH_3 had some impact on the noise intensity, but only at the lowest considered concentrations of NO_2. However, considering the changes in DC resistance, the situation is less clear (Fig. 7b). NO_2 gas dominates the sensor DC resistance only at low concentrations of NH_3. When a concentration of NH_3 exceeds 5 ppm, we observe an opposite direction of DC resistance changes induced by NO_2 increase. This means that the contrary effects of these two gases on the DC resistance of the sensor reduce the possibility of gas mixture identification to some limits of concentrations. Better results of gas mixture components identification can be expected when the sensor is additionally modulated (*e.g.*, by UV irradiation of various optical powers or wavelengths) to secure more data for the considered detection algorithms. Such an approach was successfully applied to gas sensors elsewhere using support vector machine (SVM) or other machine learning algorithms [29–31]. As an example, the SVM algorithm classifies data by finding the most optimum hyperplane to maximize the distance between different classes of data; it can also be used for regression models. SVM can be very efficient for high dimensional spaces (as in the case of the FES method) and when there is a nonlinear dependence between the variables (*e.g.*, noise intensity and gas concentration).

We applied detection algorithms to determine gas mixture components by the considered gas sensor, using the data of DC resistances (9 values for the considered NO_2 and NH_3 concentrations but excluding the cases for zero concentrations of NO_2 or NH_3 – see Fig. 7) and noise power spectral densities (9 functions $S_R(f)/R_S^2 \times f$ in the selected subband 2–20 Hz). We excluded seven measurement points in Fig. 7 (no presence of NO_2, NH_3, or both gases) because these data were biased by a drift visible in measurement time. We suppose that there is a slow diffusion process that is better visible at low concentrations of the considered gases. However, it should be reduced when the sensor thickness is optimized, and the sensor is effectively refreshed between consecutive measurements. More details on the used detection algorithms, are described in Supplementary Material.

Exemplary results for detecting gas mixture components are presented in Fig. 8. As we mentioned above, NO_2 is determined mainly by noise power spectral density, and NH_3 is determined mainly by DC resistance in the considered range of gas concentrations 2–10 ppm. Therefore, we investigated NO_2 detection at the random error of noise power spectra estimation increased by 10 % ($k = 100$, random error equals 100 %/sqrt(k) [32], Fig. 8a), and NH_3 detection at DC resistance error increased by 1 % (Fig. 8b). The results suggest that NO_2 and NH_3 can be detected in a gas mixture by a single WS_2 sensor utilizing DC resistance and its fluctuations (power spectral density of resistance fluctuations) but at their limited concentration range. The worked-out detection model is robust against measurement errors but only to some extent. We conclude that a single WS_2 gas sensor can determine gas components (NO_2 and NH_3) of the considered gas mixture at selected concentrations. Still, these conclusions cannot be transferred to other mixtures.

4. Conclusions

We demonstrated an ink-printed WS_2 sensor for UV-assisted detection of two gases of opposite redox properties (oxidizing NO_2 and reducing NH_3). We presented the prospect of utilizing measurements of both DC and random components of resistance toward gas detection. The effect of UV light on the surface of the WS_2 structure was depicted on electrical-AFM images, which showed that irradiation was responsible for amplified charge transfer and activation of the sensing surface. This had implications on sensor responses toward target gases, especially in the DC resistance response. Low-frequency noise spectra revealed that the fluctuations in the WS_2 sensor follow $1/f$-like dependence, with the noise intensity increasing proportionally to the concentration of gases. Detection limits estimated from relative changes in sensor DC resistance or noise amplitude (averaged between 2–20 Hz) were 103 ppb or 220 ppb for NO_2 and 553 ppb or 168 ppb for NH_3. Although the overall noise responses were higher than DC resistance responses, the estimation of theoretical DLs is biased by the lower accuracy of noise measurements. Still, this result can be improved by lowering the random error of the estimated noise power spectral densities using more extended measurements and longer averaging of noise data. Compared to other reports, such low limits of detection for NO_2 (hundreds or tens of ppb) were obtained before for WS_2-based sensors but either in high temperature (180 °C) [13] or for a hybrid structure that does not facilitate a simplified fabrication [25]. Comparing our sensors with those reported in recent years, we propose to use pure WS_2 material without complex fabrication procedures or structure modifications and UV light assistance at RT instead of heating. Supplementary Table A.1 summarizes and compares gas sensing devices based on WS_2 reported in recent years with the one proposed in our work.

Detecting mixtures of gases and the effect of the sensor cross-sensitivity remains an open issue. The primary observation is that the ultimate DC resistance or low-frequency noise response toward a mixture of selected concentrations is not a direct summation of the data obtained for pure gases. Therefore, the interaction between NO_2 and NH_3 during the transfer to the sensing surface or at the interface of the material must be included and requires more in-depth investigation, *e.g.*, based on computational methods. The proposed ink-printed WS_2 sensor can determine concentrations of the mixed NO_2 and NH_3 gases for a considered but limited range of their concentrations when the selected SVM algorithm is applied. The detection model is robust against measurement error to some extent. Our work presents the potential of using

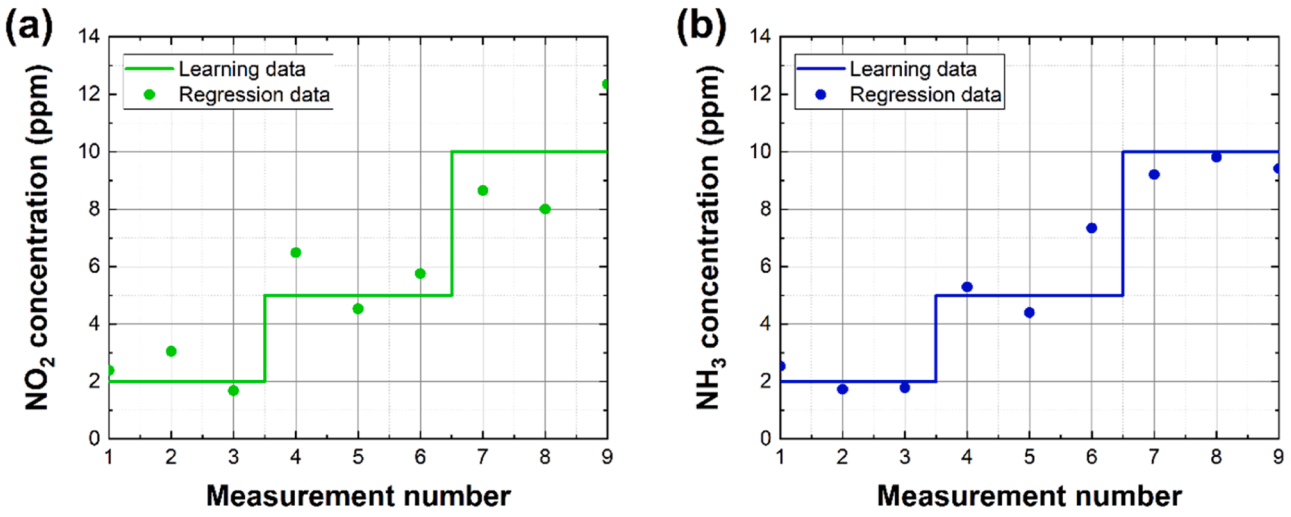

Fig. 8. Results of gas concentrations detection in gas mixture (NO_2 mixed with NH_3 in the concentrations range 2–10 ppm) for a set of 9 data records: **(a)** NO_2 when random error of the measured product $S_R(f)/R_S^2 \times f$ (in the considered range 2–20 Hz) was increased by 10 % (green dots), measurement numbers 1, 4, 7 respond to 2 ppm of NH_3, measurement numbers 2, 5, 8 respond to 5 ppm of NH_3, measurement numbers 3, 6, 9 respond to 10 ppm of NH_3; **(b)** NH_3 when random error of DC resistance R_S was increased by 1 % (blue dots), measurement numbers 1, 4, 7 respond to 2 ppm of NO_2, measurement numbers 2, 5, 8 respond to 5 ppm of NO_2, measurement numbers 3, 6, 9 respond to 10 ppm of NO_2. The algorithm *Optimizable SVM* was selected to prepare the most appropriate regression model.

ink-printed WS_2-based resistors to quantitatively detect toxic species by combining DC resistance and low-frequency noise measurements with UV light that activates detection sites (hot spots) in the WS_2 structure. Additionally, our results shed light on the possibilities of detecting mixed concentrations of target gases of opposite redox properties based on DC resistance and noise responses of the printed WS_2. We also want to highlight that although we focused on studying sensing responses to mixtures of two target gases, the effect of humidity on the DC and noise sensor response can also add an informative contribution to machine learning models. In our studies, we purposely limited the effect of RH by utilizing UV irradiation of a short wavelength (275 nm) that helps to clean the sensing surface from the preadsorbed molecules and prevents humidity from re-adsorption during gas detection. We believe the presented results are valuable for gas sensing with UV-light assistance for mixed target gases; however, the issue requires broader investigation because of additional phenomena that may occur between target gases and water molecules, specifically when the RH level changes during detection time.

CRediT authorship contribution statement

Janusz Smulko: Writing – review & editing, Writing – original draft, Supervision, Formal analysis, Conceptualization. **Katarzyna Drozdowska:** Writing – review & editing, Writing – original draft, Visualization, Resources, Investigation, Formal analysis, Data curation. **Andrzej Kwiatkowski:** Writing – review & editing, Visualization, Software, Formal analysis, Data curation. **Artur Zieliński:** Writing – review & editing, Investigation, Data curation.

Declaration of Competing Interest

The authors declare that they have no known competing financial interests or personal relationships that could have appeared to influence the work reported in this paper.

Acknowledgments

This work was funded by the National Science Centre, Poland, under the research project: 2019/35/B/ST7/02370, “System of gas detection by two-dimensional materials”.

Appendix A. Supporting information

Supplementary data associated with this article can be found in the online version at doi:10.1016/j.snb.2024.136923.

Data Availability

Data will be made available on request.

References

[1] K. Zakrzewska, Mixed oxides as gas sensors, Thin Solid Films 391 (2001).
[2] Y.Y. Broza, H. Haick, Nanomaterial-based sensors for detection of disease by volatile organic compounds, Nanomedicine 8 (2013) 785–806, https://doi.org/10.2217/nnm.13.64.
[3] E. Llobet, Gas sensors using carbon nanomaterials: a review, Sens. Actuators B Chem. 179 (2013) 32–45, https://doi.org/10.1016/j.snb.2012.11.014.
[4] X. Wang, D. Gu, X. Li, S. Lin, S. Zhao, M.N. Rumyantseva, A.M. Gaskov, Reduced graphene oxide hybridized with WS_2 nanoflakes based heterojunctions for selective ammonia sensors at room temperature, Sens. Actuators B Chem. 282 (2019) 290–299, https://doi.org/10.1016/j.snb.2018.11.080.
[5] S. Rumyantsev, G. Liu, R.A. Potyrailo, A.A. Balandin, M.S. Shur, Selective sensing of individual gases using graphene devices, IEEE Sens. J. 13 (2013) 2818–2822, https://doi.org/10.1109/jsen.2013.2251627.
[6] Q.H. Wang, K. Kalantar-Zadeh, A. Kis, J.N. Coleman, M.S. Strano, Electronics and optoelectronics of two-dimensional transition metal dichalcogenides, Nat. Nanotechnol. 7 (2012) 699–712, https://doi.org/10.1038/nnano.2012.193.
[7] A.V. Agrawal, R. Kumar, S. Venkatesan, A. Zakhidov, G. Yang, J. Bao, M. Kumar, M. Kumar, Photoactivated mixed in-plane and edge-enriched p-type MoS_2 flake-based NO_2 sensor working at room temperature, ACS Sens. 3 (2018) 998–1004, https://doi.org/10.1021/acssensors.8b00146.
[8] H. Tabata, H. Matsuyama, T. Goto, O. Kubo, M. Katayama, Visible-light-activated response originating from carrier-mobility modulation of NO_2 gas sensors based on MoS_2 monolayers, ACS Nano 15 (2021) 2542–2553, https://doi.org/10.1021/acsnano.0c06996.
[9] S. Ramu, T. Chandrakalavathi, G. Murali, K.S. Kumar, A. Sudharani, M. Ramanadha, K.R. Peta, R. Jeyalakshmi, R.P. Vijayalakshmi, UV enhanced NO gas sensing properties of the MoS_2 monolayer gas sensor, Mater. Res. Express 6 (2019), https://doi.org/10.1088/2053-1591/ab20b7.
[10] T. Pham, G. Li, E. Bekyarova, M.E. Itkis, A. Mulchandani, MoS_2-based optoelectronic gas sensor with sub-parts-per-billion limit of NO_2 gas detection, ACS Nano 13 (2019) 3196–3205, https://doi.org/10.1021/acsnano.8b08778.
[11] R. Kumar, N. Goel, M. Kumar, UV-activated MoS_2 based fast and reversible NO_2 sensor at room temperature, ACS Sens. 2 (2017) 1744–1752, https://doi.org/10.1021/acssensors.7b00731.
[12] E. Llobet, Transition metal dichalcogenide based toxic gas sensing, Curr. Opin. Environ. Sci. Heal. 37 (2024) 100533, https://doi.org/10.1016/j.coesh.2024.100533.

[13] M. Donarelli, L. Ottaviano, 2D materials for gas sensing applications: a review on graphene oxide, MoS_2, WS_2 and phosphorene, Sens. (Switz.) 18 (2018), https://doi.org/10.3390/s18113638.
[14] H.R. Gutiérrez, N. Perea-López, A.L. Elías, A. Berkdemir, B. Wang, R. Lv, F. López-Urías, V.H. Crespi, H. Terrones, M. Terrones, Extraordinary room-temperature photoluminescence in triangular WS_2 monolayers, Nano Lett. 13 (2013) 3447–3454, https://doi.org/10.1021/nl3026357.
[15] P. Wang, C. Tang, Tunable p/n property of WS_2 nanosheets-based ammonia gas sensor: assembled by drop-coating and aerosol-jet printing, Appl. Surf. Sci. 655 (2024) 1–6, https://doi.org/10.1016/j.apsusc.2024.159612.
[16] H.Y. Jun, S.J. Kim, C.H. Choi, Ink formulation and printing parameters for inkjet printing of two dimensional materials: A mini review, Nanomaterials 11 (2021), https://doi.org/10.3390/nano11123441.
[17] D.J. Finn, M. Lotya, G. Cunningham, R.J. Smith, D. McCloskey, J.F. Donegan, J. N. Coleman, Inkjet deposition of liquid-exfoliated graphene and MoS_2 nanosheets for printed device applications, J. Mater. Chem. C. 2 (2014) 925–932, https://doi.org/10.1039/c3tc31993h.
[18] M. Chen, D. Cui, N. Wang, S. Weng, Z. Zhao, F. Tian, X. Gao, K. He, C.-T. Chiang, S. Albawardi, S. Alsaggaf, G. Aljalham, M.R. Amer, C. Zhou, Inkjet-printed MoS_2 nanoplates on flexible substrates for high-performance field effect transistors and gas sensing applications, ACS Appl. Nano Mater. 6 (2023) 3236–3244, https://doi.org/10.1021/acsanm.2c04885.
[19] G. Hu, J. Kang, L.W.T. Ng, X. Zhu, R.C.T. Howe, C.G. Jones, M.C. Hersam, T. Hasan, Functional inks and printing of two-dimensional materials, Chem. Soc. Rev. 47 (2018) 3265–3300, https://doi.org/10.1039/c8cs00084k.
[20] S.G. Noyce, J.L. Doherty, S. Zauscher, A.D. Franklin, Understanding and mapping sensitivity in MoS_2 field-effect-transistor-based sensors, ACS Nano 14 (2020) 11637–11647, https://doi.org/10.1021/acsnano.0c04192.
[21] J. Smulko, G. Scandurra, K. Drozdowska, A. Kwiatkowski, Flicker Noise in Resistive Gas Sensors — Measurement Setups, Sensors 24 (2024) 1–19.
[22] K. Drozdowska, A. Rehman, A. Krajewska, D.V. Lioubtchenko, K. Pavłov, S. Rumyantsev, J. Smulko, G. Cywiński, Effects of UV light irradiation on fluctuation enhanced gas sensing by carbon nanotube networks, Sens. Actuators B Chem. 352 (2022) 131069, https://doi.org/10.1016/j.snb.2021.131069.
[23] A.A. Balandin, Low-frequency 1/f noise in graphene devices, Nat. Nanotechnol. 8 (2013) 549–555, https://doi.org/10.1038/nnano.2013.144.
[24] B. Ayhan, C. Kwan, J. Zhou, L.B. Kish, K.D. Benkstein, P.H. Rogers, S. Semancik, Fluctuation enhanced sensing (FES) with a nanostructured, semiconducting metal oxide film for gas detection and classification, Sens. Actuators, B Chem. 188 (2013) 651–660, https://doi.org/10.1016/j.snb.2013.07.056.
[25] X. Chen, J. Hu, P. Chen, M. Yin, F. Meng, Y. Zhang, UV-light-assisted NO_2 gas sensor based on WS_2/PbS heterostructures with full recoverability and reliable anti-humidity ability, Sens. Actuators B Chem. 339 (2021) 1–9, https://doi.org/10.1016/j.snb.2021.129902.
[26] X. Yan, Y. Wu, R. Li, C. Shi, R. Moro, Y. Ma, L. Ma, High-performance UV-assisted NO_2 sensor based on chemical vapor deposition graphene at room temperature, ACS Omega 4 (2019) 14179–14187, https://doi.org/10.1021/acsomega.9b00935.
[27] E. Espid, F. Taghipour, UV-LED photo-activated chemical gas sensors: a review, Crit. Rev. Solid State Mater. Sci. 42 (2017) 416–432, https://doi.org/10.1080/10408436.2016.1226161.
[28] V. Palenskis, K. Maknys, Nature of low-frequency noise in homogeneous semiconductors, Sci. Rep. 5 (2015) 1–7, https://doi.org/10.1038/srep18305.
[29] J.M. Lentka, R. Smulko, C.G. Ionescu, L.B. Granqvist, Kish, Determination of gas mixture components using fluctuation enhanced sensing and the LS-SVM regression algorithm, Metrol. Meas. Syst. 22 (2015), https://doi.org/10.1515/mms-2015-0039.
[30] M.A. Djeziri, O. Djedidi, N. Morati, J.L. Seguin, M. Bendahan, T. Contaret, A temporal-based SVM approach for the detection and identification of pollutant gases in a gas mixture, Appl. Intell. 52 (2022) 6065–6078, https://doi.org/10.1007/s10489-021-02761-0.
[31] S. Feng, F. Farha, Q. Li, Y. Wan, Y. Xu, T. Zhang, H. Ning, Review on smart gas sensing technology, Sensors 19 (2019) 1–22, https://doi.org/10.3390/s19173760.
[32] J.S. Bendat, A.G. Piersol, Random Data: Analysis and Measurement Procedures, John Wiley & Sons, 2011.

Katarzyna Drozdowska received her M.Sc. degree in nanotechnology from Gdańsk University of Technology, Poland, in 2020. During her studies, she took a traineeship at Max Planck Institute for Polymer Research, Mainz, Germany (2018), where she investigated thin-film transistors based on organic substances. Currently, she is pursuing her Ph. D. studies at the Department of Metrology and Optoelectronics in the field of electronics. She is a stipendist in one research grant and a project leader in another project on using two-dimensional materials as gas sensing components in chemiresistive sensors. Her main research focus concerns low-dimensional materials for gas sensing devices, utilizing light modulation and 1/f noise for more sensitive and selective detection of volatile compounds.

Janusz Smulko received his M.Sc., Ph.D. and D.Sc. degrees in electronics from Gdańsk University of Technology, Poland, in 1989, 1996 and 2007, respectively. Presently, he is a full professor (since 2016), Head of the Metrology and Optoelectronics Department (since 2012). He had also conducted scientific research in short-term positions at Texas A&M University (2003), Uppsala University (2006/07), Massachusetts Institute of Technology (2011, 2013). As a researcher, he focuses on the applications of 1/f noise for gas sensing and reliability assessment of electronic components and structures, the influence of noise on detection efficiency in Raman spectroscopy systems. He was Vice-Rector for Research of the Gdańsk University of Technology (in the term 2016–2019), member of the Committee on Metrology and Scientific Instrumentation of the Polish Academy of Science (two terms: 2013–2019) and Editor-in-Chief of Metrology and Measurement Systems Journal (two terms: 2013–2019), Chair of IEEE Chapter Computer Society Gdańsk (two terms: 2014–2017). Professor chaired three International Conferences on Noise and Fluctuations issues and managed seven research projects. He was a member of the H2020-MSCA-RISE-2014 project TROPSENSE: "Development of a non-invasive breath test for early diagnosis of tropical diseases" (No: 645758) and co-authored more than 140 papers.

Artur Zieliński is employed at the Department of Electrochemistry, Corrosion and Materials Science at the Faculty of Chemistry since 02/01/2005. He is engaged in research in the field of technical sciences, in the discipline of chemical technology. He obtained his doctorate on April 7, 2004, and habilitation on October 5, 2016. He is a co-author of 40 articles from the Philadelphia List, participated in 5 national and international research projects. He is the laureate of the second degree team award for outstanding scientific achievements for 2012 and 2013. The main subject of Dr. Zieliński's scientific interests is the use of scanning probe microscopy techniques in the surface analysis of structural and functional materials.

Andrzej Kwiatkowski has graduated from the Gdańsk University of Technology and defended his Ph.D. (Raman spectra processing algorithms in the process of chemical substances detection) at the Faculty of Electronics, Telecommunications, and Informatics in 2014. He published papers about data processing for chemical compounds or gas detection by signal processing methods (pre-processing methods and detection algorithms: SVM, PCA and correlation algorithms). Dr. Kwiatkowski specializes in the design and programming of embedded systems. He was involved in numerous research projects and was responsible for software preparation controlling the dedicated one-board computers (*e.g.* portable Raman spectrometer - 2011, electronic nose - 2019, exhaled breath analyzer - 2021). In 2017 and 2018, he completed a three-month internship at JLM Innovation GmbH (Tübingen, Germany), where he participated in the development of breath sample analysis devices.